

# Spontaneous symmetry breaking in dual-core baby-Skyrmion systems

Boris A. Malomed<sup>1</sup>, Yakov Shnir<sup>2,3</sup> and Gleb Zhilin<sup>4</sup>

<sup>1</sup>Department of Physical Electronics, School of Electrical Engineering,  
Faculty of Engineering, Tel Aviv University,  
Tel Aviv 69978, Israel

<sup>2</sup>Bogoliubov Laboratory for Theoretical Physics,  
Joint Institute for Nuclear Research,  
Dubna 141980, Moscow Region, Russia

<sup>3</sup>Institute of Physics  
Carl von Ossietzky University Oldenburg  
Oldenburg D-26111, Germany

<sup>4</sup>Department of Theoretical Physics and Astrophysics,  
Belarusian State University, Minsk 220004, Belarus

## Abstract

We introduce a system composed of two (2+1)-dimensional baby-skyrmion models (BSMs) set on parallel planes and linearly coupled by tunneling of fields. This system can be realized in a dual-layer ferromagnetic medium. Unlike dual-core models previously studied in nonlinear optics and BEC, here the symmetry-breaking bifurcation (SBB) in solitons (baby skyrmions) occurs with the increase of the inter-core coupling ( $\kappa$ ), rather than with its decrease, due to the fact that, even in the uncoupled system, neither core may be empty. Prior to the onset of the symmetry breaking between the two components of the solitons, they gradually separate in the opposite directions, due to the increase of  $\kappa$ , which is explained in an analytical form by means of an effective interaction potential. Such evolution scenarios are produced for originally symmetric states with topological charges in the two cores,  $B^{(1)} = B^{(2)} = 1, 2, 3, 4$ . The evolution of mixed states, of the  $(B^{(1)}, B^{(2)}) = (1, 2)$  and  $(2, 4)$  types, with the variation of  $\kappa$  is studied too.

## 1 Introduction

Diverse models of the field theory support topological solitons. Many such models have been intensively studied over last decades in a wide variety of physical contexts. Perhaps one of the simplest examples is a modified version of the non-linear  $O(3)$   $\sigma$ -model in  $(2+1)$  dimensions (the so-called “baby-skyrmion model”, BSM) [1, 2]. This is a low-dimensional simplified theory which emulates the conventional Skyrme model in  $(3+1)$  dimensions [3] in many respects, and finds direct physical realizations. In particular, hexagonal lattices of two-dimensional skyrmions were observed in a thin ferromagnetic layer [4], and in a metallic itinerant-electron magnet, where the skyrmion lattice was detected by results of neutron scattering [5], and through a specific contribution to the topological quantum Hall effect [6].

According to the Derrick’s theorem [7], to support the solitons’ stability, the Lagrangian of the BSM should include, apart from the usual  $O(3)$  sigma-model’s kinetic term, also an interaction

term quartic in derivatives<sup>1</sup>, and the potential one, which does not contain derivatives. Although the structure of the potential term is largely arbitrary, its particular choice determines different ways of symmetry breaking [8, 9, 10].

In various branches of physics, complex systems, involving several coupled scalar field, arise (see, e.g., Refs. [12, 13, 14, 15]). Properties of solitons in these extended models may be quite different from a straightforward extension of the single-component counterpart. In particular, the extended models can support non-topological solitons [12, 15].

Currently, there is a number of experimentally relevant multicomponent systems, including those in non-conventional superconductivity models (see a topical issue on this topic [16]), where a few superconducting bands and a set of corresponding Josephson coupling constants between the condensates appear. The systems of the latter type give rise to effective chiral  $CP^2$  planar skyrmions, which were constructed in the three-component Ginzburg-Landau model with broken time-reversal symmetry [17]. These configurations are actually bound states of triplets of vortices, the system being symmetric with respect to the dihedral group. It is also relevant to mention a recent experimental observation of a bound state of two magnetic baby-skyrmions, and their current-driven motion, in layered manganites [18].

In this work we introduce a system composed of two replicas of the usual  $(2 + 1)$ -dimensional BSM, set in two parallel planes (“cores”), which are linearly coupled by hopping (tunneling) between them. The fields in the two cores are also referred to below as “sectors” of the coupled system. Depending on the coupling strength, this dual system may manifest various symmetries and symmetry-breaking scenarios. A system of this type may be realized, in particular, in a bilayer ferromagnetic film, with the BSM implemented in each layer.

Linearly coupled dual-core systems with nonlinearities in each core, alias *nonlinear couplers* [19], were studied in detail in relatively simple models of nonlinear optics and Bose-Einstein condensates (BEC), represented by a single complex field in each core, which obey the respective nonlinear Schrödinger (NLS) or Gross-Pitaevskii (GP) equations. If the intrinsic nonlinearity in the cores is strong enough, the power exchange between them is effected by the intensity of the guided waves, which is used for the design of all-optical switching devices [20]. In addition to the simplest dual-core system with the cubic nonlinearity and single component in each core, realizations of nonlinear couplers have been studied in many other settings, including the bimodal propagation of light [21], twin-core Bragg gratings [22], [23], lossy optical couplers embedded into a gain medium [24], systems with saturable [25], quadratic [26, 27], cubic-quintic (CQ) [28], and nonlocal [31] nonlinearities, dual-core traps for BEC [29], parallel coupled arrays of discrete waveguides [30],  $(2 + 1)$ -dimensional couplers for spatiotemporal “light bullets” in planar dual-core waveguides [32], and  $\mathcal{PT}$ -symmetric nonlinear couplers, both  $(1 + 1)$ -dimensional [33] and  $(2 + 1)$ -dimensional [34]. Note that the  $(2 + 1)$ -dimensional dual-core waveguides have the same geometric dimension as the dual-core BSM introduced in the present work.

A fundamental property of nonlinear couplers is the symmetry-breaking bifurcation (SBB), which destabilizes obvious symmetric states in the system and gives rise to asymmetric ones. The SBB was analyzed for spatially uniform states [35] and solitons in twin-core waveguides [36], as well as for gap solitons in Bragg gratings [22] with the cubic nonlinearity (these results were originally reviewed in Ref. [37], and later in Ref. [38]). The SBB was studied too for solitons supported by the quadratic [26] and CQ [28] nonlinearities.

In all the above-mentioned systems, the study of the spontaneous symmetry breaking followed the pattern which assumed that, in the limit case of the uncoupled system, one core would carry a usual single-component soliton, while the other one is empty. Then, with the increase of the coupling constant,  $\kappa$ , the originally empty core is filled by the field tunneling from the mate core. Eventually, only symmetric states, featuring identical soliton components in both cores, exist above a critical value of  $\kappa$ , while below that value symmetric states are unstable, being replaced by stable asymmetric ones. The principal difference of the situation in the dual-core BSM considered below is that neither core is supposed to be empty, due to the boundary conditions imposed on the fields

<sup>1</sup>Recently, some modification of the BSM with the Dzyaloshinskii-Moriya interaction term was suggested to model noncentrosymmetric ferromagnetic planar structures [11].

at infinity. Therefore, it gives rise to an altogether different scenario of the symmetry breaking, with identical configurations in the uncoupled cores, which start to separate in opposite (lateral) directions, and eventually undergo an SBB, with the *increase* (rather than decrease) of  $\kappa$ ; however, at critical value  $\kappa = \kappa_{\text{cr}}$  given below by Eq. (12), the coupling cannot stabilize the baby skyrmion in the system.

The rest of the paper is structured as follows. In the next section we briefly review the model which support non-trivial soliton configurations of the dual-core BSM. Numerical results are presented in Section 3, where we consider various patterns of the evolution of the coupled configurations in two different cases, *viz.*, the “old” BSM [2] and the “new” double-vacuum model [39]. For the sake of compactness, we restrict the analysis to configurations with topological charge  $\leq 4$  in each sector. Conclusions and remarks are formulated in Section 4.

## 2 The model

As said above, we consider a set of two coupled replicas of the nonlinear modified  $O(3)$   $\sigma$ -model with the Skyrme term in  $(2+1)$  dimensions (i.e., the BSM), which is based on the following Lagrangian density:

$$\begin{aligned} L &= \sum_{a=1,2} L_a + L_{\text{coupling}}, \\ L_a &= \frac{1}{2} \partial_\mu \phi^{(a)} \cdot \partial^\mu \phi^{(a)} - \frac{1}{4} \left( \partial_\mu \phi^{(a)} \times \partial_\nu \phi^{(a)} \right)^2 - U \left( \phi^{(a)} \right), \\ L_{\text{coupling}} &= \kappa \phi_3^{(1)} \phi_1^{(2)}, \end{aligned} \quad (1)$$

where  $\phi^{(a)} = (\phi_1^{(a)}, \phi_2^{(a)}, \phi_3^{(a)})$ ,  $a = 1, 2$ , are two vectorial triplets of scalar fields which are subject to constraint

$$|\phi^{(1,2)}|^2 = 1. \quad (2)$$

Note that rescaling of the two-component model does not allow us to absorb all the constants into rescaled parameters of the potentials. Here we focus on three most essential coefficients of the model, *viz.*, two mass parameters  $\mu_{1,2}$ , which are defined below, and inter-core coupling constant  $\kappa$ .

The “skew” form of the coupling potential,  $L_{\text{coupling}}$ , which is defined in Eq. (1), is the one which gives rise to the symmetry breaking, see below. If, instead, a “straight” form is taken, with  $L_{\text{coupling}} = \kappa \phi_3^{(1)} \phi_3^{(2)}$ , it will not give rise to any symmetry breaking.

We consider fields  $\phi^{(a)}$  as maps,  $\phi^{(a)} : \mathbb{R}^2 \rightarrow S^2$ , which are characterized by two integers (topological charges),  $B^{(a)} = \pi_2(S^2)$ . Explicitly, they are given as integrals of vectorial products,

$$B^{(a)} = \frac{1}{4\pi} \iint \phi^{(a)} \cdot \left( \partial_1 \phi^{(a)} \times \partial_2 \phi^{(a)} \right) dx dy, \quad (3)$$

thus the two-component configuration possesses topological charges in both cores, that will be referred to as  $(B^{(1)}, B^{(2)})$ . Note that the symmetry of the configuration with respect to the reflections in the internal space,  $\phi_2^{(a)} \rightarrow -\phi_2^{(a)}$ , which inverts of the sign of the topological charge of the corresponding constituent, allows us to restrict the consideration to positive values of  $B^{(1,2)}$ .

In the decoupled limit,  $\kappa \rightarrow 0$ , each component approaches the vacuum value at the infinitely remote spatial boundary in the respective two-dimensional plane. This boundary value is commonly taken as  $\phi_\infty^{(1,2)} = (0, 0, 1)$ , thus an  $O(3)$ -symmetry-breaking potential,  $U(\phi^{(a)})$ , which vanishes at the boundary, stabilizes the configuration. In the dual-core system, we can relax the restriction on the asymptotic value of one component, say  $\phi_\infty^{(2)}$ . For the fields taking values on the unit sphere, as per Eq. (2), we assume

$$\phi_\infty^{(1)} = (0, 0, 1), \quad (4)$$

which provides the one-point compactification of the spatial boundary.

The explicit form of potential  $U(\phi^{(a)})$  is largely arbitrary. There are a few familiar examples, such as the BSM with the so-called “old” potential [2],

$$U(\phi^{(a)}) = \mu_a^2 [1 - \phi_3^{(a)}], \quad (5)$$

which corresponds to the unique vacuum of component  $\phi^{(a)}$ , or the double-vacuum model [39], with

$$U(\phi^{(a)}) = \mu_a^2 [1 - (\phi_3^{(a)})^2]. \quad (6)$$

Both potentials are invariant with respect to iso-rotations about the third component  $\phi_3^{(a)}$ , hence at  $\kappa = 0$  the symmetry of the model is broken<sup>2</sup> to  $SO(2) \times SO(2)$ . On the other hand, the vacuum structure strongly depends on the value of the inter-core coupling,  $\kappa$ , as the coupling term in (1) violates the rotational invariance, and it can completely break the symmetry.

Note that the structure of the potential term is important for the stability. For example, iso-rotations of skyrmions with topological charge  $B$  in the model with the “old” potential may break them into  $B$  skyrmions with charge 1 [41].

The violation of the rotational invariance in the BSM has recently drawn a great deal of attention. It was demonstrated that the effect strongly depends on the particular choice of the above-mentioned potential [8, 9, 10]. Here we consider another symmetry-breaking mechanism, introduced by the linear coupling between the cores carrying the two sectors of systems. As mentioned above, this mechanism was previously studied in detail in systems of linearly coupled NLS/GP equations.

First we consider the model with the double vacuum potentials in each sector, hence the total potential is

$$U(\phi^{(1)}, \phi^{(2)}) = \mu_1^2 [1 - (\phi_3^{(1)})^2] + \mu_2^2 [1 - (\phi_3^{(2)})^2] + \kappa \phi_3^{(1)} \phi_1^{(2)}. \quad (7)$$

Evidently, the coupling between the sectors may stabilize the configuration when both mass parameters  $\mu_1, \mu_2$  are zero.

### 3 Numerical results

#### 3.1 States with the equal topological charges in the two sectors

In this section results produced by numerical solutions are presented for the dual-core BSM. The solutions were chiefly constructed on an equidistant grid in polar coordinates  $(\rho, \theta)$ , employing the compactified radial coordinate,

$$\xi = \rho/(1 + \rho) \in [0, 1], \quad (8)$$

and  $\theta \in [0, 2\pi]$ , i.e.  $x = \rho \sin \theta$ ,  $y = \rho \cos \theta$ . To find minima of the functional corresponding to Lagrangian density (1), we have implemented a simple forward-differencing scheme on a square lattice with spacing  $\Delta x = 0.01$ . Typically, the grids of size  $120 \times 120$  were used, the relative errors of the final solutions being  $\lesssim 10^{-4}$ . To check our results for the correctness, we evaluated the values of the topological charges of the components by direct integration of expressions (3).

Initial configurations were taken as per the straightforward hedgehog ansatz,

$$\phi_1^{(a)} = \sin(f(\rho)) \cos(B^{(a)}\theta), \quad \phi_2^{(a)} = \sin(f(\rho)) \sin(B^{(a)}\theta), \quad \phi_3^{(a)} = \cos(f(\rho)), \quad (9)$$

where the input profile function is  $f(\rho) = 4 \arctan(e^{-\rho})$ . Evidently, this corresponds to the configuration with topological charge  $B^{(a)}$  and standard boundary conditions (b.c.) imposed on the profile function,  $f(\rho)$ , in both sectors of the dual-core system (1). Note that ansatz (9) is

---

<sup>2</sup>In the double vacuum model, there is an additional reflection symmetry,  $Z_2 \times Z_2$ .



rotationally invariant, because the spatial  $SO(2)$  rotation about the  $z$ -axis is equivalent to the  $O(2)$  iso-rotation about component  $\phi_3^{(a)}$ . However, in our calculations we do not adopt any *a priori* assumptions about spatial symmetries of components of the field configuration,  $\phi^{(a)}$ .

As said above [see Eq. (4)], for component  $\phi^{(1)}$  b.c. is chosen as

$$\phi_1^{(1)} \Big|_{\rho \rightarrow \infty} \rightarrow 0, \quad \phi_2^{(1)} \Big|_{\rho \rightarrow \infty} \rightarrow 0, \quad \phi_3^{(1)} \Big|_{\rho \rightarrow \infty} \rightarrow 1, \quad (10)$$

while the second component is subject to b.c.

$$\partial_\rho \phi_1^{(2)} \Big|_{\rho \rightarrow \infty} \rightarrow 0, \quad \phi_2^{(2)} \Big|_{\rho \rightarrow \infty} \rightarrow 0, \quad \partial_\rho \phi_3^{(2)} \Big|_{\rho \rightarrow \infty} \rightarrow 0. \quad (11)$$

Then, the total potential energy of system (7) can be minimized. Indeed, b.c. (10), (11), along with the restriction of the fields to the unit sphere [Eq. (2)], demonstrates that, as  $\rho \rightarrow \infty$ , the potential tends to  $U(\phi^{(1)}, \phi^{(2)})_\infty = \mu_2^2 (\phi_1^{(2)})^2 + \kappa \phi_1^{(2)}$ , thus the originally unknown asymptotic values of the components  $\phi_1^{(2)}$  and  $\phi_3^{(2)}$  depend on mass parameter  $\mu_2$  and coupling constant  $\kappa$ .

Furthermore, the total asymptotic potential possess a minimum if  $\phi_1^{(2)}|_\infty = -\kappa/(2\mu_2^2) \in [-1, 1]$ . We fix the scales by setting  $\mu_2 = 1$ , hence there is a critical value of the coupling,

$$\kappa_{\text{cr}} = 2. \quad (12)$$

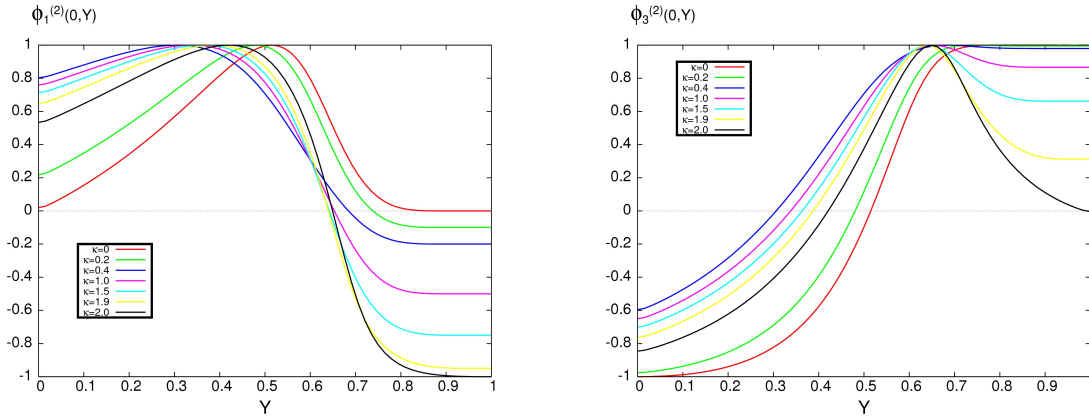


Figure 1: (Color online) Field components  $\phi_1^{(2)}$  and  $\phi_3^{(2)}$  of the  $(1,1)$  configuration along the positive  $y$  axis compactified onto the unit interval,  $Y = y/(1+y) \in [0, 1]$ , cf. Eq. (8), in the model with potential (7) at  $\kappa = 0; 0.2; 0.4; 1.0; 1.5; 1.9; 2.0$ .

Indeed, it is seen in Fig. 1, which displays components  $\phi_1^{(2)}$  and  $\phi_3^{(2)}$  of the  $(B^{(1)}, B^{(2)}) = (1, 1)$  configurations along the compactified  $y$  axis, for some set of values of coupling  $\kappa$ , that, as the coupling approaches the critical value (12), the asymptotic behavior of component  $\phi_3^{(2)}$  becomes different, ceasing to decay exponentially. Thus, in this limit the total potential cannot stabilize the corresponding baby skyrmion in the second sector, where the mode becomes unstable with respect to radiation of scalar radiation waves.

As the coupling increases above the critical value (12), the configuration again gets stabilized. Eventually, at large  $\kappa$  the fields approach the vacuum values at a finite distance from the center, and their asymptotic values cease to vary.

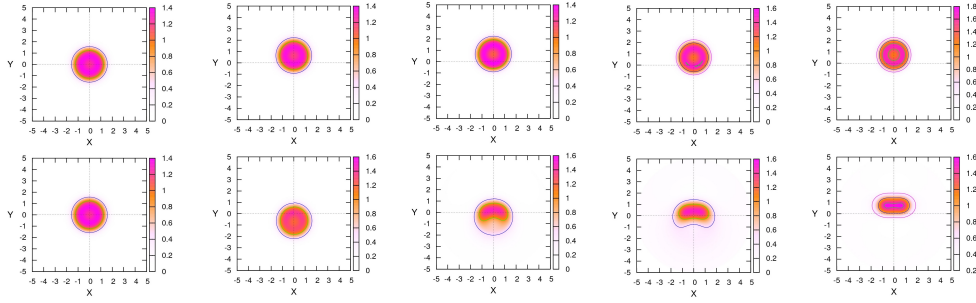


Figure 2: (Color online) The upper and lower rows display contour plots of the energy density in the two sectors of the  $(1,1)$  configuration in the model with potential (7) at  $\kappa = 0, 0.1, 1.0, 1.5, 2.0$  (from left to right).

Hereafter, we restrict the consideration for the coupled BSMs with fixed values of the mass parameters,  $\mu_1 = \mu_2 = 1$ , unless stated otherwise (recall  $\mu_2 = 1$  was already fixed above), and coupling constant  $\kappa$  gradually increasing from zero. In Figs. 2-9 we present the so found contour plots of the energy densities in the two sectors of the system, given by functions  $L_1(x, y)$  and  $L_2(x, y)$ , and the coupled field components,  $\phi_1^{(2)}$ ,  $\phi_3^{(1)}$ , which illustrate typical configurations of the  $(B^{(1)}, B^{(2)}) = (1, 1), (2, 2), (3, 3)$  and  $(4, 4)$  types.

First, we consider in detail the simplest configuration, of the  $(1,1)$  type. As the inter-core coupling,  $\kappa$ , increases, the components in the two cores rapidly start to separate, the distance between them attaining a maximum at  $\kappa \approx 0.15$ . This distance is, actually, slightly smaller than the size of the charge-1 baby skyrmion, as seen in the second row of Fig. 2.

To explain this observation, we note that the coupling remains weak, and the components in this regime are almost undeformed, which suggests to evaluate the effective potential of the interaction between the two components as a function of the separation between them. To this end, following the well-known approach adopted in the perturbation theory for solitons [42], we take unperturbed baby skyrmions of unit charge in the two cores, separated by distance  $d$  in the lateral direction, and calculate the corresponding interaction potential of the  $(1,1)$  configuration:

$$U_{\text{int}}(d) = \kappa \iint \phi_3^{(1)} \left( x, y + \frac{d}{2} \right) \phi_1^{(2)} \left( x, y - \frac{d}{2} \right) dx dy \quad (13)$$

Numerical evaluation shows that this potential has a minimum at  $d = -1.4$ , see the right plot in Fig. 10, which clearly explains the spontaneous separation between the components.

When coupling becomes stronger, the asymptotic values of the components  $\phi_1^{(2)}$  and  $\phi_3^{(2)}$  start to vary and the constituents begin to deform. The baby skyrmion in the first sector with  $B^{(1)} = 1$  remains almost rotationally invariant, with a small local minimum of the energy density at the

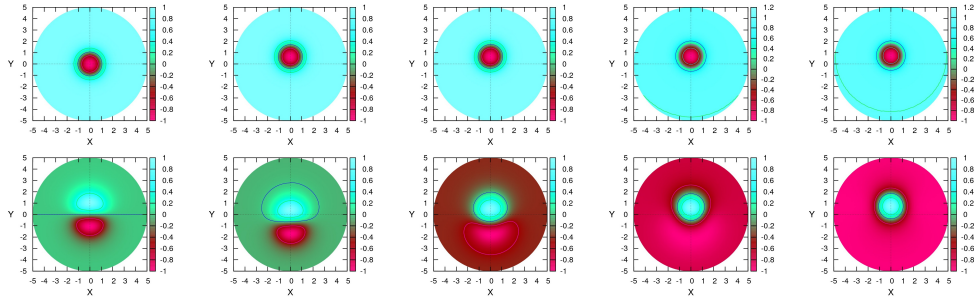


Figure 3: (Color online) Contour plots of coupled components  $\phi_3^{(1)}$  and  $\phi_1^{(2)}$  (the upper and lower rows, respectively) of the (1,1) configuration in the model with potential (7) at  $\kappa = 0, 0.1, 0.8, 1.5, 2.0$  (from left to right).

soliton's center, while the soliton with  $B^{(2)} = 1$  in the second sector features broken rotational invariance, see the third row in Figs. 2 and 1. This transition from the separated but intrinsically symmetric configuration to the one with the broken symmetry between the components of the state of the (1,1) type is a specific realization of the SBB in the present system. Below, realizations of the SBB in configurations of the (2,2), (3,3) and (4,4) types are presented too.

Further increase of the coupling leads to breaking of the rotational symmetry of the skyrmion in the first sector too, and it becomes symmetric with respect to the reflection,  $x \rightarrow -x$ . Finally, as the coupling constant approaches the critical value (12), components  $\phi_1^{(2)}$  and  $\phi_3^{(2)}$  swap their roles, as shown in Fig. 1. Indeed, the strong coupling between component  $\phi_3^{(1)}$  in the first sector, which is subject to the fixed vacuum-asymptotic behavior,  $\phi_3^{(1)} \rightarrow -1$  at  $\rho = 0$  and  $\phi_3^{(1)} \rightarrow 1$  as  $\rho \rightarrow \infty$ , and the “flexible” component in the second sector,  $\phi_1^{(2)}$ , forces the latter one to interpolate between the “upper” vacuum value,  $\phi_1^{(2)} \rightarrow 1$ , at the origin, and the “lower” vacuum value,  $\phi_1^{(2)} \rightarrow -1$ , as  $\rho \rightarrow \infty$ . As the asymptotic behavior of component  $\phi_2^{(2)}$  is fixed, in this limit configuration components  $\phi_1^{(2)}$  and  $\phi_3^{(2)}$  are actually swapped.

In the left plot of Fig. 10, we represent the results of the analysis of the SBB in the systematic form, displaying the inter-core symmetry-breaking energy measure,

$$\Delta = \left( E^{(2)} - E^{(1)} \right) / \left( E^{(2)} + E^{(1)} \right), \quad (14)$$

where  $E^{(a)} = \iint L_a dx dy$  is defined as per Eq. (1), as a function of the coupling constant,  $\kappa$ , for the static configurations with identical topological charges in both sectors.

Evidently, the asymmetry is growing from zero to a maximal value which corresponds to the critical coupling (12). Note that the asymmetry between the sectors decreases with the increase of the common topological charge of both sectors.

In the uncoupled double-vacuum system, the baby skyrmions are always rotationally invariant. As the coupling strength,  $\kappa$ , increases, the symmetry gets broken and the norm of the soliton in the second sector grows faster, as its symmetry is lower. When the coupling approaches the critical

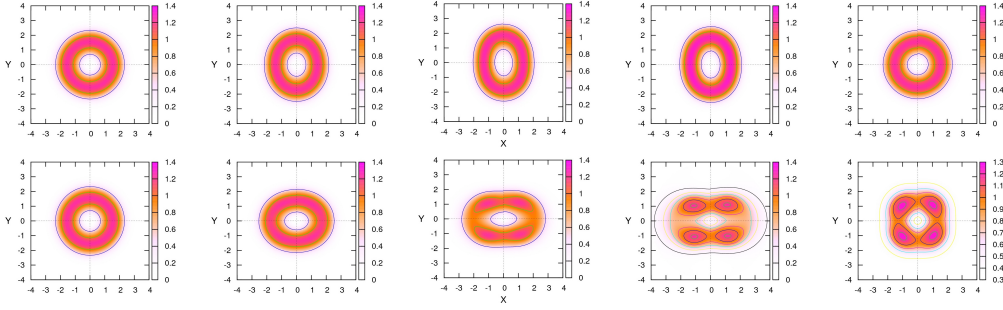


Figure 4: (Color online) Contour plots of the energy density of the sectors in the  $(2, 2)$  configuration in the model with potential (7) at  $\kappa = 0, 0.2, 0.7, 1.0, 2.0$  (from left to right).

value (12), the charge-1 soliton in the first sector regains the rotational invariance, featuring an annular shape of its energy-density distribution. On the other hand, the second sector is composed of two segments, featuring the discrete dihedral  $D_2$  symmetry, similar to the solutions presented in Ref. [8] in the single-component model with an  $O(2)$ -symmetry-breaking potential,  $U(\phi) = \mu^2(1 - \phi_3^2)(1 - \phi_1^2)$ , cf. Eq. (7). Further increase of  $\kappa$  almost does not affect the asymptotic values of the fields, the asymmetry between the components remaining nearly constant; however as mentioned above, in that limit the baby skyrmions are, in fact, compactons, with the fields reaching the vacuum values at a finite distance from the center of the configuration.

### 3.2 States with different topological charges in the sectors and other forms of the coupling

The pattern of the evolution of the coupled configuration with different topological charges, following the increase of  $\kappa$ , is somewhat different from what is outlined above. In Figs. 11, 12 and 13, 14 we display contour plots for the energy-density distributions in the coupled components of the  $(1, 2)$  and  $(2, 4)$  configurations, respectively, for a set of values of  $\kappa$ .

Unlike the configuration  $(1, 1)$  that we considered above, the increase of  $\kappa$  from the initial zero value does not cause displacement of the components from their initial positions. Instead, they start to break the rotationally symmetric shapes in each sector, evolving towards two different  $D_2$ -symmetric solitons stretched along the  $y$ - and  $x$ -axes in the first and second sectors, respectively, see the second row in Fig. 11. As the coupling becomes stronger and  $\kappa$  increases above a certain value close to 1, the dihedral  $D_2$  symmetry of the soliton in the second sector breaks down, and two pairs of segments emerge in this charge-2 component. Similar to the pattern reported above for the  $(1, 1)$  configuration, at the critical value (12) of the coupling constant, components  $\phi_1^{(2)}$  and  $\phi_3^{(2)}$  actually swap,  $\kappa$  playing the role of the angle of the iso-rotation of the configuration in the second sector about component  $\phi_2^{(2)}$ . The final configuration then consist of a charge-1 rotationally invariant skyrmion in the first sector, with an annular shape of the energy-density distribution, and a charge-2 skyrmion with discrete dihedral  $D_4$  symmetry in the second sector.

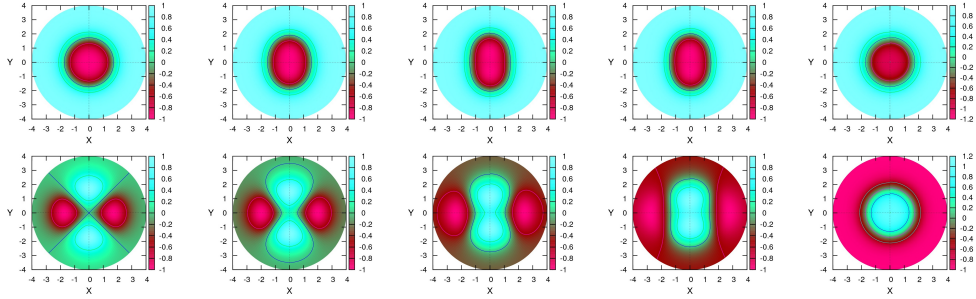


Figure 5: (Color online) Contour plots of coupled components  $\phi_3^{(1)}$  and  $\phi_1^{(2)}$  (the upper and lower rows, respectively) of the (2,2) configuration in the model with potential (7) at  $\kappa = 0, 0.2, 0.7, 1.0, 2.0$  (from left to right).

Similar evolution scenarios were observed for configurations with higher charges. To summarize those results, we mention that the evolution of the  $(n, m)$  configuration in the model with potential (7) starts from the rotationally invariant configurations in both sectors. As the coupling,  $\kappa$ , increases, the energy-density distributions in both components become polygonal, i.e., symmetric with respect to dihedral group  $D_m$  with symmetry axes of different orders. The further increase of  $\kappa$  induces the permutation of the asymptotic forms of components  $\phi_1^{(2)}$  and  $\phi_3^{(2)}$ , and the configuration approaches the critical limit when the first component with topological charge  $B^{(1)} = n$  regains the rotational invariance, while the second component with charge  $B^{(2)} = m$  is shaped as a necklace built of  $2m$  half-skyrmions, which is symmetric with respect to dihedral group  $D_{2m}$ . In particular, exactly this scenario is observed for configurations of (2, 2), (3, 3), (2, 4) and (4, 4) types in Figs. 4, 6, 8 and 14.

Some additional remarks are necessary here. Firstly, as mass parameters  $\mu_1$  and  $\mu_2$  of potential (7) are vanishing, the asymmetry between the sectors vanishes too, the configurations in both sectors getting rotationally invariant for all values of  $\kappa$ , see Fig. 15. In that case, the system is stable due to the coupling between the sectors, the coupling constant is unbounded from above, there being no critical value of  $\kappa$  [cf. Eq. (12)], and norms in both sectors increase equally with the subsequent growth of  $\kappa$ , hence the asymmetry does not change anymore. Furthermore, the coupling can stabilize the system even when the mass parameters take negative values.

Secondly, for the model with “old” potential (5), the general evolution scenario is similar to that in the model with the double vacuum potential (7) considered above, although some peculiarities may differ. To demonstrate that, we briefly consider model (1) with potential

$$U(\phi^{(1)}, \phi^{(2)}) = \mu_1^2 \left[ 1 - (\phi_3^{(1)})^2 \right] + \mu_2^2 \left[ 1 - (\phi_3^{(2)})^2 \right] + \kappa \phi_3^{(1)} \phi_1^{(2)}. \quad (15)$$

In the numerical solution, we fix the mass parameters as above,  $\mu_1 = \mu_2 = 1$ , and let the coupling constant,  $\kappa$ , gradually increase from zero. Then, in Figs. 16-18 we display contour plots of the energy density, which illustrate a typical scenario of the evolution of configurations (1, 1), (2, 2) and (3, 3) in the model with potential (15), cf. similar plots in Figs. 2, 4 and 6. Once again, the

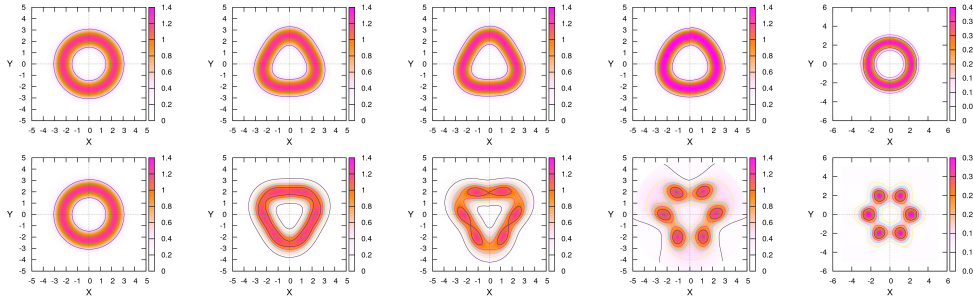


Figure 6: (Color online) Contour plots of the energy density of the sectors in the  $(3, 3)$  configuration in the model with potential (7) at  $\kappa = 0, 0.4, 0.8, 1.5, 2.0$  (from left to right).

$(1, 1)$  configuration in the weak-coupling regime exhibits separation of the components without their deformations, see Fig. 16. However as coupling becomes stronger, some novelty is observed. The difference from the model with the double vacuum potential (7) is that, depending on values of masses  $\mu_{1,2}$ , the configurations with topological charge  $B^{(1,2)} \geq 2$  may not possess the initial rotational invariance [40]. Accordingly, the symmetry breaking evolves differently, two distinct steps being identified in the evolution of the coupled configuration. At first, similar to the model with potential (7), as  $\kappa$  increases from zero, the energy-density distributions of both components become symmetric with respect to dihedral group  $D_m$ , with symmetry axes of different orders. However, as the coupling grows stronger, at  $\kappa > 1$  the asymptotic forms of components  $\phi_1^{(2)}$  and  $\phi_3^{(2)}$  are not completely swapped, and the configuration approaches another critical limit, when the first component with topological charge  $B^{(1)} = n$  again restores the rotational invariance, while the second component with topological charge  $B^{(2)} = m$  is formed as a set of  $m$  individual charge-1 skyrmions, which is symmetric with respect to dihedral group  $D_m$ , hence the number of the respective segments is twice as small as in the model with the potential (7).

Thus, the above results depend on the choice of the symmetry-breaking interaction potential, such as those given by Eq. (7) and (15). Other options for inducing symmetry breaking are also possible. In particular, while the above-mentioned “straight” coupling, of the form of  $\kappa\phi_3^{(1)}\phi_3^{(2)}$ , in Eq. (1) does not, by itself, break the symmetry between the two cores, it can be demonstrated that the linear-coupling potential chosen as  $\kappa\phi_1^{(1)}\phi_2^{(2)}$  leads to a completely different pattern of the symmetry breaking in the dual-core system.

Another interesting possibility is to consider the “skew-symmetrized” form of the coupling potential

$$L_{\text{coupling}} = \kappa \left( \phi_3^{(1)} \phi_1^{(2)} + \phi_1^{(1)} \phi_3^{(2)} \right)$$

and impose identical boundary conditions (11) in both sectors to allow the transformation of components  $\phi_1^{(1)}$  and  $\phi_3^{(1)}$  too. Then, as  $\kappa$  increases from zero, the initial rotational invariance of both components of the  $(m, m)$  configuration gradually becomes broken to dihedral group  $D_{2m}$  with symmetry axes of the same orders.

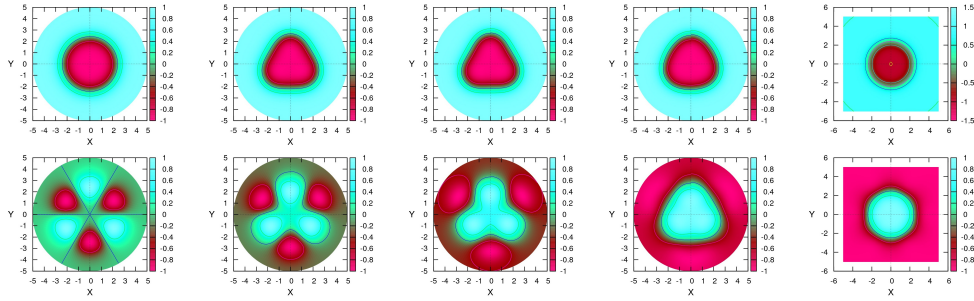


Figure 7: (Color online) Contour plots of coupled components  $\phi_3^{(1)}$  and  $\phi_1^{(2)}$  (the upper and lower rows, respectively) of the (3,3) configuration in the model with potential (7) at  $\kappa = 0, 0.4, 0.8, 1.5, 2.0$  (from left to right).

Finally, it can be demonstrated that the coupling of the soliton component with a topologically trivial field in the second sector yields a non-topological soliton (lump), whose structure precisely matches the distribution of the coupling energy. In this configuration, only one component of the field in the second sector,  $\phi_1^{(2)}$ , is nontrivial at  $\kappa > 0$ .

## 4 Conclusions

The objective of this work is to introduce a class of dual-core  $(2 + 1)$ -dimensional field-theory models, such as the BSM (baby Skyrme model). Each skyrmion resides in its plane (core), the two parallel planes being related by linear tunneling of the fields. This model can be implemented in dual-layer magnetic media. As in previously studied dual-core models of nonlinear optics and BEC, the interplay of the intra-core nonlinearity and linear inter-core coupling ( $\kappa$ ) gives rise to the SBB (symmetry-breaking bifurcation) of the solitons, but, on the contrary to those models, where the SBB occurs with the decrease of  $\kappa$ , in the present system it takes place with the increase of  $\kappa$ , which is explained by the fact that cores cannot be empty even at  $\kappa = 0$ . The SBB follows the initial increase of the lateral separation between the two components without the symmetry breaking, which is caused by the increase of  $\kappa$  from zero, and was explained by means of the effective potential of the interaction between the two components. These evolution scenarios were studied for different species of the two-component baby skyrmions, categorized by values of the topological charge in the components: initially symmetric ones, of the (1,1), (2,2), (3,3), and (4,4) types, and asymmetric composite states, (1,2) and (2,4).

## Acknowledgments

This work was financially supported by Alexander von Humboldt Foundation in the framework of the Institutes linkage Programm. Ya.S. and G.Z. are grateful to the Institute of Physics at



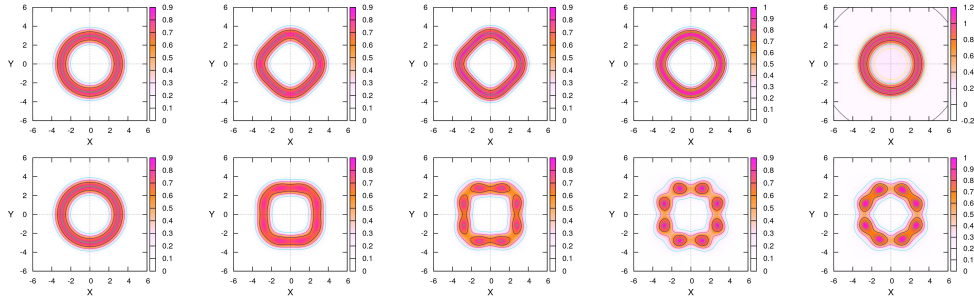


Figure 8: (Color online) Contour plots of the energy density of the components of the  $(4,4)$  configuration in the model with potential (7) at  $\kappa = 0, 0.4, 0.8, 1.5, 2.0$  (from left to right).

the Carl von Ossietzky University Oldenburg for hospitality. We thank Marek Karliner for useful discussions.

## References

- [1] A. A. Bogolubskaya and I. L. Bogolubsky, Phys. Lett. A **136** (1989) 485;  
A. A. Bogolubskaya and I. L. Bogolubsky, Lett. Math. Phys. **19** (1990) 171.
- [2] B. M. A. Piette, W. J. Zakrzewski, H. J. W. Mueller-Kirsten, D. H. Tchrakian, Phys. Lett. B **320** (1994) 294.  
B. M. A. Piette, B. J. Schroers, W. J. Zakrzewski, Z. Phys. C **65** (1995) 165.
- [3] T. H. R. Skyrme, Proc. Roy. Soc. A **260** (1961) 127.
- [4] X. Z. Yu, Y. Onose, N. Kanazawa, J. H. Park, J. H. Han, Y. Matsui, N. Nagaosa, and Y. Tokura, Nature **465** (2010) 901.
- [5] S. Mühlbauer, B. Binz, F. Jonietz, C. Pfleiderer, A. Rosch, A. Neubauer, R. Georgii, and P. Böni, Science **323** (2009) 915.
- [6] A. Neubauer, C. Pfleiderer, B. Binz, A. Rosch, R. Ritz, P. G. Niklowitz, and P. Böni, Phys. Rev. Lett. **102** (2009) 186602.
- [7] G. H. Derrick, J. Math. Phys. **5** (1964) 1252.
- [8] R. S. Ward, Nonlinearity **17** (2004) 1033.
- [9] I. Hen, M. Karliner, Nonlinearity **21** (2008) 399.
- [10] J. Jäykkä., M. Speight and P. Sutcliffe, Proc. Roy. Soc. Lond. A **468** (2012) 1085.



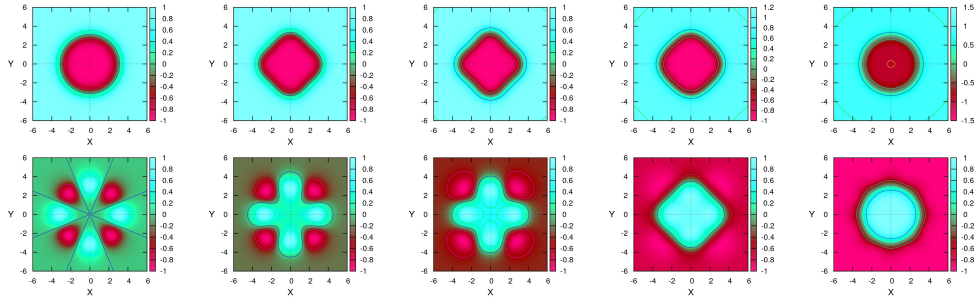


Figure 9: (Color online) Contour plots of coupled components  $\phi_3^{(1)}$  and  $\phi_1^{(2)}$  (the upper and lower rows, respectively) of the (4,4) configuration in the model with potential (7) at  $\kappa = 0, 0.4, 0.8, 1.5, 2.0$  (from left to right).

- [11] A. N. Bogdanov and D. A. Yablonsky, Sov. Phys. JETP **95** (1989) 178; A. N. Bogdanov, JETP Lett **62** (1995) 247.
- [12] R. Rajaraman, Phys. Rev. Lett. **42** (1979) 200.
- [13] D. Bazeia, M. J. dos Santos and R. F. Ribeiro, Phys. Lett. A **208** (1995) 84; arXiv:hep-th/0311265.
- [14] B. A. Malomed and A. A. Nepomnyashchy, Europhys. Lett. **27** (1994) 649.
- [15] A. Halavanau, T. Romanczukiewicz, and Y. Shnir, Phys. Rev. D **86** (2012) 085027 [arXiv:1206.4471 [hep-th]].
- [16] P. C. W. Chu, A. Koshelev, W. Kwok, I. Mazin, U. Welp, and H.-H. Wen. (Eds.), Physica C **469** (2009) 313 .
- [17] J. Garaud, J. Carlstrom, E. Babaev and M. Speight, Phys. Rev. B **87** (2013) 014507; arXiv:1211.4342.
- [18] X. Z. Yu, Y. Tokunaga, Y. Kaneko, W. Z. Zhang, K. Kimoto, Y. Matsui, Y. Taguchi, and Y. Tokura, Nature Commun. **5** (2014) 3198.
- [19] S. M. Jensen, IEEE Journal of Quantum Electr. **18** (1982) 1580; A. A. Maier, Sov. J. Quant. Electron. **12** (1982) 1490.
- [20] S. R. Friberg, Y. Silberberg, M. K. Oliver, M. J. Andrejco, M. A. Saifi, and P. W. Smith, Appl. Phys. Lett. **51** (1987) 1135; D. R. Heatley, E. M. Wright, and G. I. Stegeman, *ibid.* **53** (1988) 172 ; I. M. Uzunov, R. Muschall, M. Göllés, Yu. S. Kivshar, B. A. Malomed, and F. Lederer, Phys. Rev. E **51** (1995) 2527; W. Królikowski and Y. S. Kivshar, J. Opt. Soc. Am. B **13** (1996) 876; S. C. Tsang, K. S. Chiang, and K. W. Chow, Opt. Commun. **229** (2004) 431; D. Chevriaux, R. Khomeriki, and J. Leon, Mod. Phys. Lett. B **20** (2006) 515.

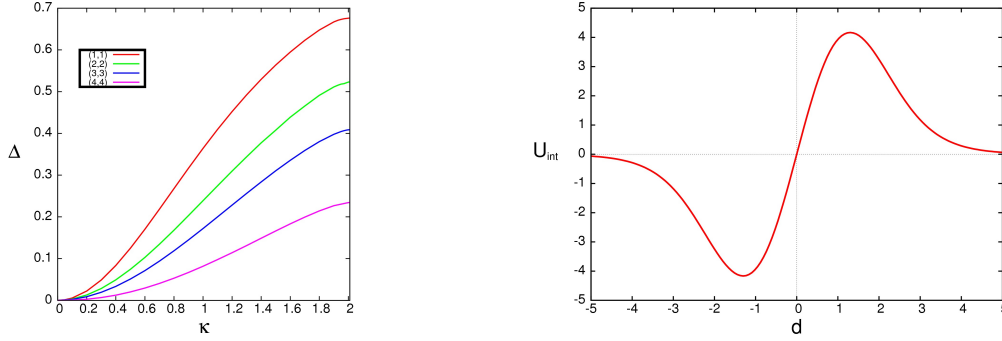


Figure 10: (Color online) Left: The symmetry measure, defined as per Eq. (14), for the (1, 1), (2, 2), (3, 3) and (4, 4) configurations, versus the coupling constant,  $\kappa$ . Right: The effective potential of interaction between the components of the (1, 1) configuration, defined as per Eq. (13), versus the separation between them,  $d$ .

- [21] S. Trillo and S. Wabnitz, J. Opt. Soc. Am. **B** 5 (1988) 483.
- [22] W. C. K. Mak, B. A. Malomed, and P. L. Chu, J. Opt. Soc. Am. B **15** (1998) 1685.
- [23] Y. J. Tsofe and B. A. Malomed, Phys. Rev. E **75** (2007) 056603; Y. Sun, T. P. White, and A. A. Sukhorukov, J. Opt. Soc. Am. B **30** (2013) 736.
- [24] N. V. Alexeeva, I. V. Barashenkov, K. Rayanov, and S. Flach, Phys. Rev. A **89** (2014) 013848.
- [25] G. D. Peng, P. L. Chu, and A. Ankiewicz, Int. J. Nonlin. Opt. Phys. **3** (1994) 69.
- [26] W. C. K. Mak, B. A. Malomed, and P. L. Chu, Phys. Rev. E **55** (1997) 6134.
- [27] A. Shapira, N. Voloch-Bloch, B. A. Malomed, and A. Arie, J. Opt. Soc. Am. B **28** (2011) 1481.
- [28] L. Albuch, B. A. Malomed, Math. Comput. Simul. **74** (2007) 312.
- [29] A. Gubeskys and B. A. Malomed, Phys. Rev. A **75** (2007) 063602 ; M. Matuszewski, B. A. Malomed, and M. Trippenbach, *ibid.* **75** (2007) 063621; L. Salasnich, B. A. Malomed, and F. Toigo, *ibid.* **81** (2010) 045603 .
- [30] G. Herring, P. G. Kevrekidis, B. A. Malomed, R. Carretero-González, and D. J. Frantzeskakis, Phys. Rev. E **76** (2007) 066606; Lj. Hadžievski, G. Gligorić, A. Maluckov, and B. A. Malomed, Phys. Rev. A **82** (2010) 033806; X. Shi, F. Ye, B. Malomed, and X. Chen, Opt. Lett. **38** (2013) 1064.

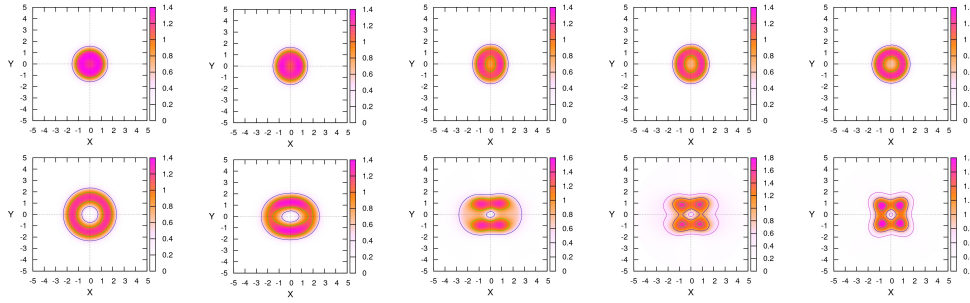


Figure 11: (Color online) Contour plots of the energy density of the sectors in the  $(1, 2)$  configuration in the model with potential (7) at  $\kappa = 0, 0.4, 1.0, 1.5, 2.0$  (from left to right).

- [31] X. Shi, B. A. Malomed, F. Ye, and X. Chen, Phys. Rev. A **85** (2012) 053839.
- [32] N. Dror and B. A. Malomed, Physica D **240** (2011) 526.
- [33] R. Driben and B. A. Malomed, Opt. Lett. **36** (2011) 4323; N. V. Alexeeva, I. V. Barashenkov, A. A. Sukhorukov, and Y. S. Kivshar, Phys. Rev. A **85** (2012) 063837.
- [34] G. Burlak and B. A. Malomed, Phys. Rev. E **88** (2013) 062904.
- [35] A. W. Snyder, D. J. Mitchell, L. Poladian, D. R. Rowland, and Y. Chen, J. Opt. Soc. Am. B **8** (1991) 2102.
- [36] E. M. Wright, G. I. Stegeman, S. Wabnitz, Phys. Rev. A **40** (1989) 4455 ; C. Paré and M. Florjańczyk, Phys. Rev. A **41** (1990) 6287; A. I. Maimistov, Sov. J. Quant. Electr. **21** (1991) 687; P. L. Chu, B. A. Malomed, and G. D. Peng, J. Opt. Soc. Am. B **10** (1993) 1379; N. Akhmediev and A. Ankiewicz, Phys. Rev. Lett. **70** (1993) 2395; J. M. Soto-Crespo and N. Akhmediev, Phys. Rev. E **48**, 4710(1993); K. S. Chiang, Opt. Lett. **20** (1995) 997; B. A. Malomed, I. M. Skinner, P. L. Chu, and G. D. Peng, Phys. Rev. E **53** (1996) 4084.
- [37] M. Romagnoli, S. Trillo and S. Wabnitz, Opt. Quantum Electron. **24** (1992) S1237.
- [38] B. A. Malomed, in: Progr. Optics **43**, 71(E. Wolf, editor: North Holland, Amsterdam, 2002).
- [39] T. Weidig, Nonlinearity **12** (1999) 1489.
- [40] B. M. A. Piette, B. J. Schroers, W. J. Zakrzewski, Nucl. Phys. B **439** (1995) 205.
- [41] R. Battye, M. Haberichter, Phys. Rev. D **88** (2013); 125016 [arXiv:1309.3907 [hep-th]]  
A. Halavanau and Ya. Shnir, Phys. Rev. D **88** (2013) 085028 (8pp);
- [42] Y. S. Kivshar and B. A. Malomed, Rev. Mod. Phys. **61** (1989) 763.

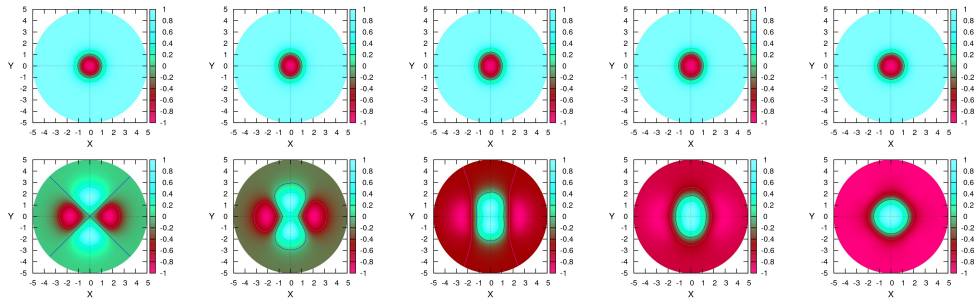


Figure 12: (Color online) Contour plots of coupled components  $\phi_3^{(1)}$  and  $\phi_1^{(2)}$  (the upper and lower rows, respectively) of the (1,2) configuration in the model with potential (7) at  $\kappa = 0, 0.4, 1.0, 1.5, 2.0$  (from left to right).

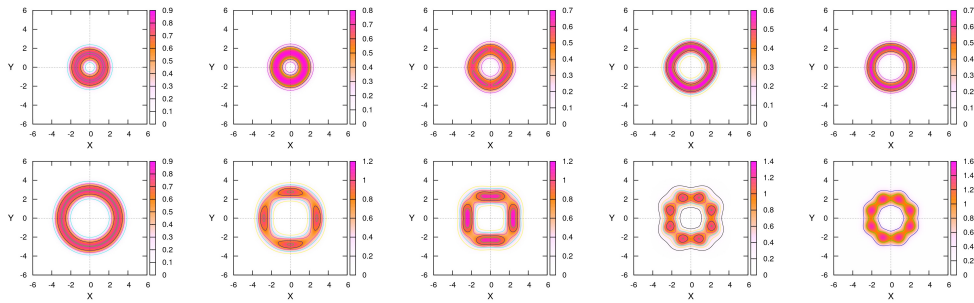


Figure 13: (Color online) Contour plots of the energy density of the sectors of the (2,4) configuration in the model with potential (7) at  $\kappa = 0, 0.4, 0.8, 1.5, 2.0$  (from left to right).

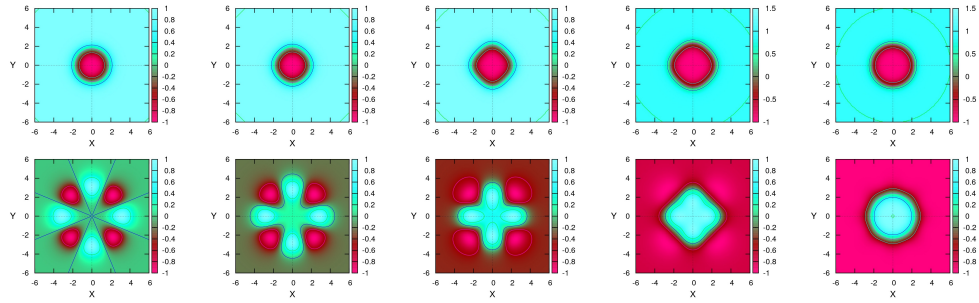


Figure 14: (Color online) Contour plots of coupled components  $\phi_3^{(1)}$  and  $\phi_1^{(2)}$  (the upper and lower rows, respectively) of the (2,4) configuration in the model with potential (7), at  $\kappa = 0, 0.4, 0.8, 1.5, 2.0$  (from left to right).

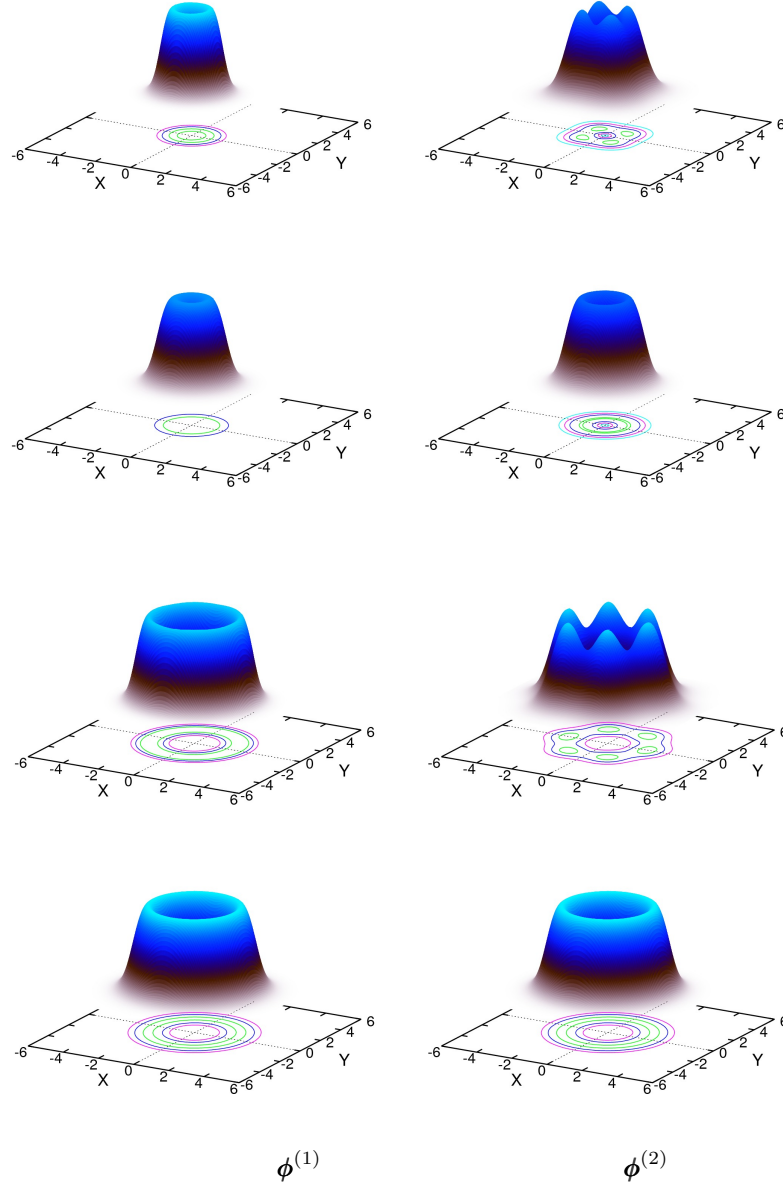


Figure 15: (Color online) Energy density plots of the two components in the (1,2) and (3,3) configurations (the top and bottom panels, respectively) for  $\kappa = 2$ , in the model with potential (7) and  $\mu_1 = \mu_2 = 1$  (the first and third rows), or  $\mu_1 = \mu_2 = 0$  (the second and forth rows).

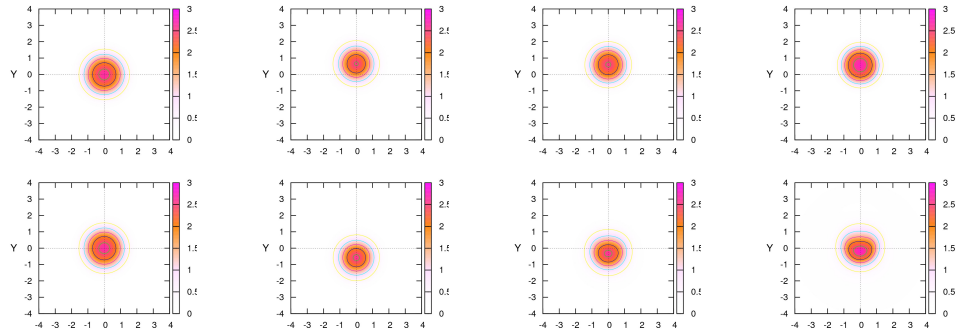


Figure 16: (Color online) Contour plots of the energy density of the components of the (1,1) configuration in the model with potential (15), at  $\kappa = 0, 0.2, 1.0, 2.0$  (from left to right).

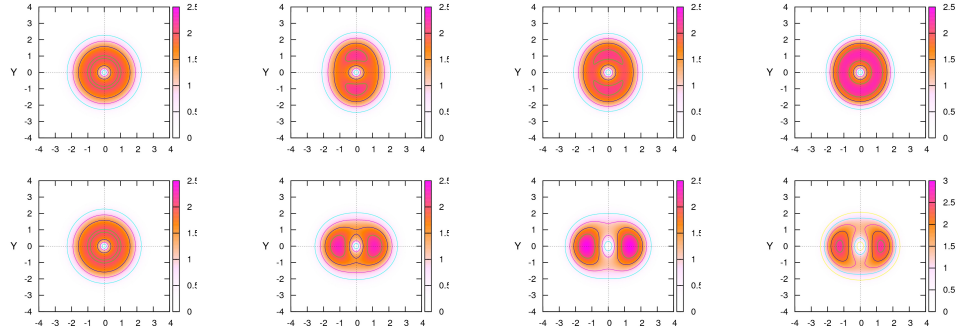


Figure 17: (Color online) The energy density of components of the  $(2,2)$  configuration in the model with potential (15), at  $\kappa = 0, 0.2, 1.0, 2.0$  (from left to right).

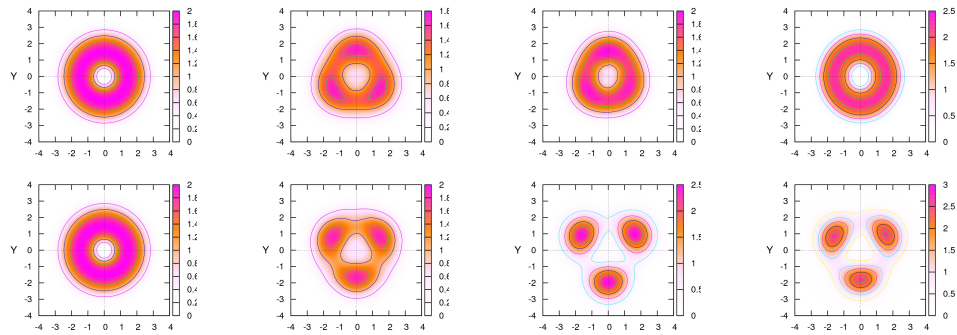


Figure 18: (Color online) The energy density of components of the  $(3,3)$  configuration in the model with potential (15), at  $\kappa = 0, 0.3, 1.0, 2.0$  (from left to right).